16TH EUROPEAN CONFERENCE ON EARTHQUAKE ENGINEERING THESSALONIKI 18 - 21 JUNE 2018

STUDY OF THE SPATIAL CORRELATION OF EARTHQUAKE GROUND MOTION BY MEANS OF PHYSICS-BASED NUMERICAL SCENARIOS

Maria INFANTINO[1], Roberto PAOLUCCI[2], Chiara SMERZINI[3], Marco STUPAZZINI[4]

ABSTRACT

Spatial correlation of the ground motion plays a key role in all those applications requiring the definition of the joint occurrence of ground motion intensities at several locations during the same earthquakes, such as in seismic risk assessment of portfolios of buildings or spatially distributed infrastructure systems in large urban areas. In spite the increasing amount of strong-motion records in recent years, the overall number of near source records (i.e. Rrup < 5-10 km) remains extremely limited. For this reason, the strong ground motion in this region may be insufficiently constrained in spite of its importance for a proper assessment of the potential losses. Therefore, in this study we decided to take advantage of the 3D physics-based numerical simulations (3DPBNSs) demonstrating their capability to reproduce the spatial correlation of the recorded earthquake ground motion. Geostatistical tools are used to this end. Four different case studies worldwide have been considered: Po Plain (Northern Italy), Thessaloniki (Greece), Beijing (China) and Istanbul (Turkey). The locations share the following features: (i) proximity to a well-known mapped fault capable to trigger a severe earthquake, (ii) a relatively good description of the geotechnical characterization of the soil and (iii) a reliable reconstruction of the deep alluvial structure. The results obtained are compared against the real ones computed using the large set of stations which recorded the 2012 Po Plain earthquake and against some previously published studies on this topic. The results 3DPBNSs-based were found consistent with the empirical ones demonstrating that numerical simulations can realistically represent the real correlation structures at long and short periods.

Keywords: spatial correlation; physics-based earthquake scenarios; near field; seismic risk assessment

1. INTRODUCTION

The description of the ground motion scaling and attenuation plays a key role in the seismic hazard assessment. Ground motion prediction equations (GMPEs), relations derived empirically from strong motion databases of past earthquakes that define the distribution of expected ground motion intensity measures as a function of magnitude, site parameters and distance from the source, are traditionally used to this end. In most cases, GMPEs are an effective tool, relatively simple, easy to use and requiring limited computational resources. However, GMPEs have several drawbacks that cannot be disregarded. One of the most critical limitations is that GMPEs cannot reproduce the spatial correlation of the ground motion, which is crucial in all those applications requiring the definition of the joint occurrence of ground motion intensities at several locations during the same earthquakes, such as in seismic risk assessment of portfolios of buildings or spatially distributed infrastructure systems in large urban areas (Hong 2000; Park et al. 2007; Weatherill et al. 2015). To overcome this problem, several spatial correlation models, which provide the intersite separation distance beyond which a given ground motion

[1]PhD Student, Department of Civil and Environmental Engineering, Politecnico di Milano, Milan, Italy, maria.infantino@polimi.it
[2]Department of Civil and Environmental Engineering, Politecnico di Milano, Milan, Italy, roberto.paolucci@polimi.it
[3]Department of Civil and Environmental Engineering, Politecnico di Milano, Milan, Italy, chiara.smerzini@polimi.it
[4]Munich RE, München, Germany, MStupazzini@munichre.com

intensity measure can be considered uncorrelated, have been proposed. More specifically, some studies analyze the recordings of a single earthquake (e.g., Boore et al. 2003; Wang and Takada 2005; Jayaram and Baker 2009) while other consider observations from multiple earthquakes (e.g. Goda and Hong 2008a; Goda and Atkinson 2009; Goda and Atkinson 2010; Sokolov et al. 2010; Esposito and Iervolino 2011 and 2012).

In recent years, stimulated by the increasing development of high performance computing, 3D physics-based numerical simulations (3DPNBSs) have emerged as a powerful complementary (or alternative) tool to the classic GMPEs-based approach to provide more detailed ground motion predictions during real as well as future, realistic earthquakes. 3DPBNSs allow to model for a specific region all factors that affect earthquake ground motion and that are not properly captured with GMPEs, furthermore they make feasible the study of a multi-scale simulation from the seismic source to the structural response within a single computational model (Mazzieri et al. 2013; Isbiliroglu et al. 2015). Thus, 3DPBNSs are particularly important in regions with limited (or non-existent) observational databanks and also for site-specific investigations, where the importance of different assumptions on the input parameters can be studied (Douglas and Aochi 2008). Several authors demonstrated the effectiveness of 3DPBSs at global (Graves 1996; Wald and Graves 1998; Pitarka et al. 1998; Komatitsch and Tromp 2002a,b) and regional (Bao et al. 1998; Olsen 2000; Dumbser and Käser 2006; Day et al. 2008; Tsuda et al. 2011; Smerzini and Villani 2012; Taborda and Bielak 2014; Villani et al. 2014; Paolucci et al. 2015; Chaljub et al. 2015; Gatti et al. 2017) scale. Nevertheless, in spite of the advantages of using the numerical simulations, some drawbacks have been always pointed out as a reasonable justification to limit the use of this kind of methodology only to few selected case study. More specifically, the main drawbacks of such an approach are related to: (i) the high level of detail of input data required; (ii) computational cost due to the large size of the 3D mesh; (iii) complexity to perform such simulations (expert users needed); (iv) the range of frequencies over which numerical results are reliable is most often limited to 1or 1.5 Hz. In order to overcome the latter limitation, broad-band (BB) waveforms are generally obtained by means of a hybrid approach, which consists of gluing low-frequency results from 3DPBNSs with high-frequency signals from stochastic approaches. Despite its wide applications, the hybrid approach suffers also from some relevant drawbacks due to the incapability of reproducing a realistic spatial correlation of the ground motion at short period. In this sense, an efficient method based on the use of Artificial Neural Networks (ANN) has been proposed by Paolucci et al. (2017) and, as a major outcome, was found to produce the actual spatial correlation of peak values of ground motion both at short and long period. This procedure will be referred to as ANN2BB in the following.

This paper aims at evaluating the spatial correlation of broadband 3DPBNSs, considering different spectral ordinates, both at short and long periods. Four different case studies worldwide have been considered: Po Plain (Northern Italy), Thessaloniki (Greece), Beijing (China) and Istanbul (Turkey). The locations share the following features: (i) proximity to a well-known mapped fault capable to trigger a severe earthquake, (ii) a relatively good description of the geotechnical characterization of the soil and (iii) a reliable reconstruction of the deep alluvial structure. These simulations have been carried out using the numerical code SPEED (http://speed.mox.polimi.it/), already successfully applied to other case studies (e.g. Stupazzini et al., 2009; Chaljub et al., 2010, Smerzini and Villani, 2012; Evangelista et al., 2017, Pilz et al., 2011, Guidotti et al., 2011, Paolucci et al., 2015, Paolucci et al., 2016) and naturally designed to tackle large-scale seismic wave propagation problems including the coupled effects of a seismic fault rupture, the propagation path through Earth's layers and localized geological irregularities such as alluvial basins and topographic relieves (Mazzieri et al. 2013).

The work is organized as follows. After having introduced the geostatistical tool used to evaluate the spatial correlation, the main results are presented. More specifically, first, the 29 May 2012 Po Plain earthquake, for which a wide set of near-source recordings at small to intermediate separation distances is available, is taken as validation case study to compare the spatial correlation estimates from 3DPBNSs with the observed ones. Secondly, the results obtained for the four cases are discussed and compared against some previously published works on this topic.

2. OVERVIEW OF GEOSTATISTICS: ESTIMATING SEMIVARIOGRAMS

This section briefly introduces the geostatistical tools commonly used in seismology and in other fields

to describe the spatial correlation of a random function. Let us consider a spatially distributed random function $Z(\mathbf{x}) = (Z_{x1}, Z_{x2}, \ldots, Z_{xi}, \ldots, Z_{xn})$, where Z_{xi} is the random variable considered at the site *i* located at the place x_i. Random variables are spatially correlated at some scale and it can be quantified by means of the semivariogram γ, a geostatistical tool that describes the average dissimilarity of two random variables as follows:

$$\gamma(Z_{xi}, Z_{xj}) = \frac{1}{2} Var(Z_{xi} - Z_{xj}) = \frac{1}{2} E\left[\{Z_{xi} - Z_{xj}\}^2\right] \quad (1)$$

Where *Var* and *E* denote the variance and expected value respectively. Residuals of ground motion intensity measures within a set of sites for a given earthquake are regarded as spatial random variables. For each site, however, we do not have multiple realizations of a given earthquake, making it impossible to draw inferences from it. Consequently, to overcome this limitation, researchers generally work under the hypothesis of stationarity: the random function $Z(\mathbf{x})$ is assumed a second-order (or weaker) stationary process, which implies: (i) the expected value of the random variable Z_x is constant across space: $E(Z_x) = \mu$, where μ is constant; (ii) the covariance depends only on the separation distance vector **h**: $C(\mathbf{h}) = cov(Z_x, Z_{x+\mathbf{h}})$, where $C(\mathbf{h})$ is independent of *x*.
With the second-order stationary assumption the semivariogram depends only on the separation vector **h** and covariance and semivariogram are equivalent:

$$\gamma(\mathbf{h}) = \frac{1}{2} Var(Z_x - Z_{x+\mathbf{h}}) = \frac{1}{2} E[\{Z_x - Z_{x+\mathbf{h}}\}^2] \quad (2)$$

$$\gamma(\mathbf{h}) = C(\mathbf{0}) - C(\mathbf{h}) = \sigma^2 - C(\mathbf{h}) \quad (3)$$

Where $C(\mathbf{0}) = \sigma^2$ is the variance of Z_x. Moreover, we can introduce the spatial correlation coefficient defined as:

$$\rho(\mathbf{h}) = \frac{C(\mathbf{h})}{\sigma^2} = 1 - \frac{\gamma(\mathbf{h})}{\sigma^2} \quad (4)$$

Modeling the spatial correlation with semivariograms is generally carried out by the following steps: (i) calculation of the sample semivariogram $\hat{\gamma}(\mathbf{h})$ from the data set; (ii) selection of the proper semivariogram model fitting the data; (iii) estimation of the parameters for the chosen model.
Referring to the first point, the sample semivariogram is estimated through the method of moments (Matheron 1965):

$$\hat{\gamma}(\mathbf{h}) = \frac{1}{2N(\mathbf{h})} \sum_{j=1}^{N(\mathbf{h})} \{z_{x_j} - z_{x_j+\mathbf{h}}\}^2 \quad (5)$$

where $z_{x_j} - z_{x_j+\mathbf{h}}$ is the difference between the data at sites separated by $\mathbf{h}$ and $N(\mathbf{h})$ denotes the total numbers of pairs at lag $\mathbf{h}$. It is worth mentioning that the sample semivariogram can be computed using the more robust estimator proposed by Cressie and Hawkins (1980), less sensitive to the outliers. However, in this study, as in other similar works (e.g. Jayaram and Baker 2009; Loth and Baker 2011), the formulation of Matheron (1965) (Equation 5) is used. Once that sample semivariogram is computed, a functional form (negative definite) fitting the data has to be selected. The basic models generally used to this end are the Exponential, Gaussian or Spherical models defined for an isotropic case (i.e. the vector distance $\mathbf{h}$ is replaced by a scalar *h*) respectively by the Equations 6, 7 and 8 (see Figure 1).

$$\gamma(h) = a\left[1 - \exp\left(-\frac{3h}{b}\right)\right] \quad (6)$$

$$\gamma(h) = a\left[1 - \exp\left(-\frac{3h^2}{b^2}\right)\right] \quad (7)$$

$$\gamma(h) = \begin{cases} a\left[\frac{3}{2}\left(\frac{h}{b}\right) - \frac{1}{2}\left(\frac{h}{b}\right)^3\right]; & if\ h \le b \\ a & ; otherwise \end{cases} \quad (8)$$

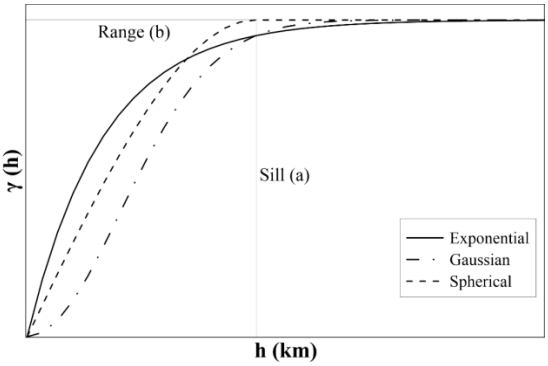

Figure 1. Semivariogram models

The parameters defininig the models, *a* and *b*, are called *sill* and *range*, and represent the variance of the random process and the separation distance at which the data can be considered fully uncorrelated, respectively.
In this work the exponential model has been used to fit visually the data starting from the least-squares regression results. Although such "manual" fitting could seem subjective, it allows to define semivariogram models that are more accurate at short distances, as explained in Jayaram and Baker (2009).

3. SPATIAL CORRELATION OF STRONG GROUND MOTION FOR SOME CASE STUDIES

The procedure introduced in the previous section allows to estimate the theoretical semivariogram, $\gamma(\boldsymbol{h})$, under the assumption of a full random process. The latter can be expressed through Equation 9, where μ is the mean (assumed to be constant) and $\varepsilon(\boldsymbol{x})$ is a random variable of zero mean and covariance $C(\boldsymbol{h})$. If the random process has a trend (i.e. a gradual variation in space), such as in the case of ground motion intensities which attenuate with distance, μ varies in a predictable manner depending on the position ($\boldsymbol{x}$), see Equation 9, and the semivariogram has to be computed using the residuals $\varepsilon(\boldsymbol{x})$ (i.e. replacing $Z_x - Z_{x+\boldsymbol{h}}$ with $\varepsilon_x - \varepsilon_{x+\boldsymbol{h}}$ in Equation 2 and 5).

$$Z(\boldsymbol{x}) = \mu(\boldsymbol{x}) + \varepsilon(\boldsymbol{x}) \quad (9)$$

In order to compute the residuals of the ground motions most of the authors (e.g. Wang and Takada 2005, Jayaram and Baker 2009, Esposito and Iervolino 2011, 2012) use the median predictions of existing ground motion prediction models. These latter predict a prescribed spectral ordinate at period *k,* at a site *s* due to the earthquake *e* and take the general form:

$$log\, Y_{sek} = log\, \bar{Y}_{sek}(M, R, S, \delta) + \eta_{ek} + \varepsilon_{sek} \quad (10)$$

where Y_{sek} denotes the ground motion intensity measure of interest; $\bar{Y}_{sek}$ is the predicted median function of magnitude (M), distance from the source (R), local-site conditions (S) and others (δ); η_{ek} is the inter-event residual which is a random variable with zero mean constant during the same earthquake across all the sites for a given period; finally ε_{sek} represents the intra-event residuals, a random variable with zero mean variable site-to-site. Thus, the spatial correlation is computed on the intra-event residuals ε_{sek}.
However, other authors (e.g., Goda and Hong 2008a; Goda and Atkinson 2009; Sokolov et al. 2010) preferred to find a regression relationship specific for the analyzed set of data and use it to compute the median estimates for residual computations. In this study the same choice has been made to avoid

dependecy issues from specific GMPEs. Thus, a simple functional form defined by Equation 11 is adopted and calibrated (using Matlab regression tools) on the specific dataset under consideration for each soil class.

$$log_{10}\bar{Y}_{sek} = c1 + log_{10}(R_{line} + c2) \quad (11)$$

where $c1$ and $c2$ are model parameters, while R_{line} is the closest distance from the surface fault projection of the segment at the top edge of the rupture plan (see definition in Hashemi et al. 2016; Paolucci et al. 2016). Consequently, spatial correlation is estimated on the logarithmic residuals computed as the misfit between the ground motion intensity values and the trend computed by means of Equation 11.

3.1 Analysis and Results

As already mentioned, the aim of this study is to investigate the spatial correlation features for different spectral ordinates using the ANN2BB broad-band results, obtained using physics-based simulations.
To this end, the analysis includes the following steps: (1) import the ANN2BB data for a selected scenario; (2) randomly select a certain number of stations N_s and compute the residuals $log_{10}Y_{sek} - log_{10}\bar{Y}_{sek}$ for each station; (3) divide the range of separation distance between the pairs of stations Δ into bins of width δ; (4) all pairs of stations that fall in the same interval are used to compute the sample semivariogram; (5) sill and range (i.e. parameters *a* and *b*) are estimated by fitting the exponential model to sample semivariogram.

3.1.1. Po Plain earthquake

The first case study thoroughly investigated is the numerical simulation of the Mw 6 Po Plain earthquake in Northern Italy occurred on 29 May 2012. This event has been selected because it provides a dataset of more than about 30 near-source strong-motion records at epicentral distances less than 30 km (Figure 4), which is very relevant for validation purposes. Moreover, the accuracy of the 3D physics-based numerical simulations in predicting the observed ground motion has been already demonstrated in Paolucci et al. (2015, 2017), to which the reader is referred for more detailed information. In the current paper we focus on the validation between simulated and recordings in terms of spatial correlation.
In this respect, Figure 2 shows the semivariograms for different spectral ordinates (PGA, SA 0.2s, SA 1.0s and SA 2.0s) computed at the available accelerometric stations (for further details see Paolucci et al. 2015) both for records and broadband simulated ground motions (ANN2BB). More specifically, diamonds and circles denotes the sample semivariograms using ANN2BB data and records (REC) respectively, while the blue solid and red dashed lines identify the corresponding exponential models. A good agreement is found between observations and synthetics, as, in both cases, the range (i.e., the distance beyond which the spatial correlation is lost) is approximately 19-25 km. The relative error between the two range estimations is bounded between 1% (for SA(0.2s)) and 20% (for PGA).

Note that the simulated ground motion intensities for T >= 0.75 s are derived entirely from the 3DPBNSs, while for T <0.75s they are the result of the ANN2BB procedure. Thus, Figure 2 highlights the ability of the ANN2BB methodology of reproducing accurately the spatial correlation structure at short spectral ordinates. Moreover, the top panels of Figure 2 (PGA and SA0.2s) show the sample semivariograms (black plus symbols) and semivariogram model (black dashed line) computed with the standard hybrid (HYB) approach in which the high-frequency contribution was obtained with Sabetta and Pugliese (1996) approach (SP96). This hybrid method produces a semivariogram which is almost flat, denoting a zero correlation coefficient at all interstation distances. Such a behavior is due to the fact the SP96 approach does not involve rigorous considerations of the physics of the earthquake, rather it produces time histories with peak ground motion values and spectral features compliant with median estimates of GMPEs. Therefore, it suffers from the inherent limits of GMPEs in reproducing the actual spatial variability of ground motion. Contrary to the ANN2BB approach where important factors affecting ground shaking, such as source directivity and site effects, described by the simulations at long periods are reflected also in the short period range, in the hybrid case the low and high frequency parts turn out to be uncorrelated, being generated through independent methods.

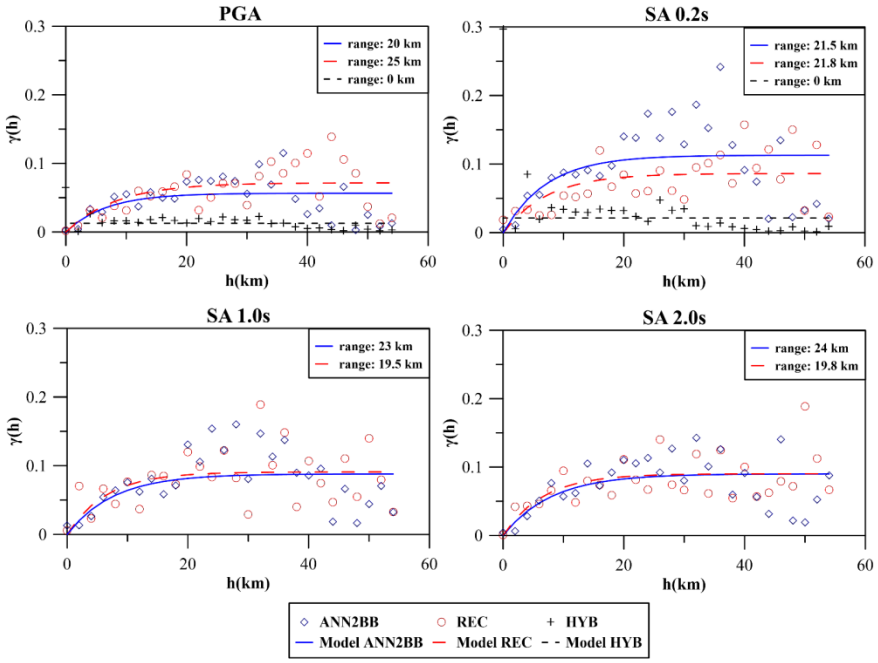

Figure 2. Semivariograms obtained using records REC (circles) and the ANN2BB approach (diamonds) for PGA (top left), SA(0.2s) (top right), SA(1.0s) (bottom left) and SA(2.0s) (bottom right). The corresponding best-fitting exponential models are denoted by continuous line and dashed line for ANN2BB and REC, respectively. Moreover, for the short period response spectral ordinates (see top panel) the semivariograms (plus symbols) and the corresponding best-fitting model from HYB results are also shown for comparison. (After Paolucci et al. 2017)

One of the remarkable advantage of using results of numerical simulations is the possibility to simulate realistic ground motions at an arbitrarily large number of sites, differently from real earthquakes, allowing to investigate potential anisotropy phenomena in the spatial correlation structure. For instance, even if the Po Plain earthquake provides one of the widest set of near-source records from moderate-to-large earthquakes worldwide, the number of records is still hardly sufficient to identify proper subsets and to investigate possible anisotropies.

Figure 3 shows the correlation models for PGA (left-hand side), and SA1.0s (right-hand side), computed by means of Equation 4 using a large set of simulated ground motions values located in the northern (black dashed line) and southern (black dot dashed line) sector with respect to the fault, specifically, at distances R_{line} lower than 10 km (N and S set, respectively). Finally, the blue solid line denotes the correlation models obtained on ANN2BB motions at the accelerometric stations considered previously. With reference to the right side of Figure 3, it is evident that for intermediate-to-long period spectral ordinates (i.e. SA 1s) the ranges are significantly shorter when only the near-fault receivers, with R_{line} < 10 km both in the North and South direction, are considered. On the other hand, at short period (left-hand side of Figure 3, referring to PGA) the decrease of the correlation with distance is less pronounced and it is evident only for the receivers lying at south of the fault projection. The rapid decay of the spatial correlation close to the fault can be directly linked to the peculiar ground motion in the near field, characterized by small-scale spatial variability associated with the heterogeneous rupture process.

3.1.2. Other case studies: Thessaloniki, Istanbul and Beijing

This section presents the spatial correlation estimates obtained for the Thessaloniki, Istanbul and Beijing physics-based numerical ground motion simulations. More specifically, the Thessaloniki simulation, presented in Smerzini et al. (2017), considers the earthquake ground motion in the Thessaloniki urban area during the destructive Mw 6.5 event occurred on June 20th 1978, better known as Volvi earthquake. On the other hand, Istanbul and Beijing simulations of Mw 7.0 and Mw. 6.5, are selected from two large set of possible earthquake ground motion scenarios simulated in order to perform seismic risk evaluations in Istanbul (Infantino, 2016) and Beijing (Antonietti et al. 2017) urban areas respectively.

Figure 4 shows the average shear-wave velocity for the upper 30 m depth ($V_{S,30}$) map, the monitors selected (black circles), the superficial projection of the active fault (red line) and epicenter (red star) for each case investigated.

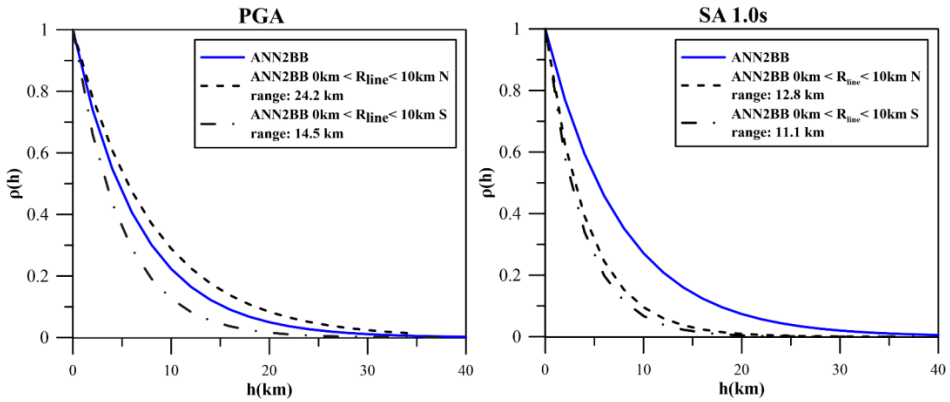

Figure 3. Correlation models obtained with ANN2BB values (blue solid line) at the considered stations. The black dash and dash dot lines show the correlation models computed using a larger number of ANN2BB receivers with R_{line} < 10 km at the Northern (N) and Southern (S) side respectively.

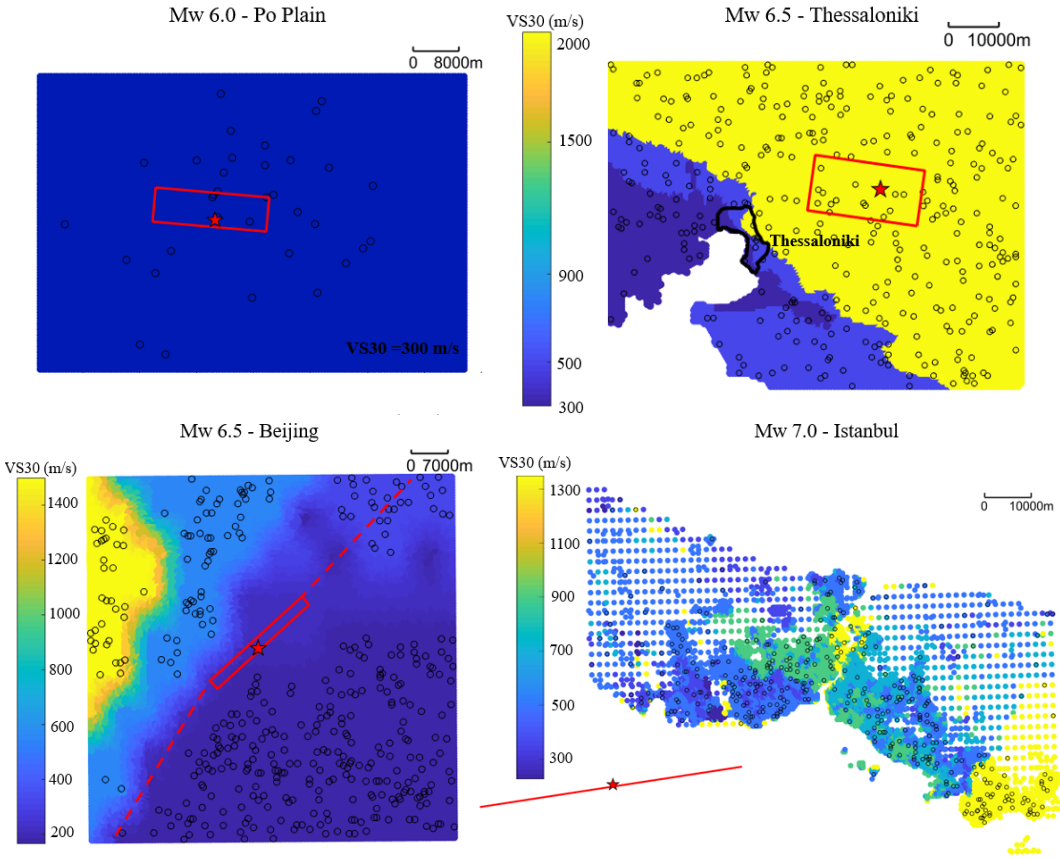

Figure 4. $V_{S,30}$ Maps, monitors selected for computing the semivariogram (black circles), superficial projection of the active fault (red line), epicenter (red star) for the Mw 6.0 Po Plain (top left), Mw 6.5 Thessaloniki (top right), Mw 6.5 Beijing (bottom left) and Mw 7.0 Istanbul (bottom right) simulations

Contrary from the Po Plain simulation described in the previous section, for the case studies presented herein observed ground motion records are not available for validation purposes. Thus, we will limit to investigate the ranges of the semivariograms obtained from the synthetics and to compare them with

other published studies. For each simulation a number of 400 monitors was randomly selected and consequently about 79800 pairs were used to estimate correlation of the geometric mean of the horizontal components for different spectral ordinates. The bin width was chosen so that there is a stable trend of correlation with at least 30 pairs per bin (Journel and Huijbregts 1978). Figure 5 shows the results for the case of Thessaloniki and for two spectral ordinates, SA(0.5s) and SA(1.0s).

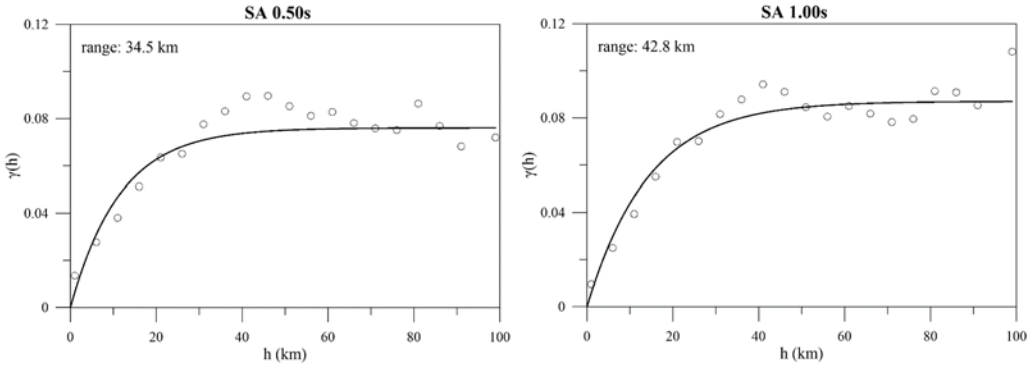

Figure 5. Sample semivariograms and fitted exponential models for the Thessaloniki simulation for SA 0.50s (left) and SA 1.0s (right).

The results of all case studies are presented in Figure 6 (filled colored dots), where the trend of range versus periods is depicted. The Po Plain results have been also included in this plot. The ranges are computed for five spectral ordinated: PGA, SA 0.2s, SA 1.0s and SA 3.5s. Moreover, the ranges estimated with independent literature studies, based on ground motion recordings, are also shown. More specifically, grey symbols refer to the ranges computed by Esposito and Iervolino (2012) using Italian Accelerometric Archive (ITACA), and the European Strong-Motion Database (ESD), while in red the ranges obtained by Jayaram and Baker (2009) using data from Anza, Alumn Rock, Parkfield, Chi-Chi, Northridge, Big Bear City and Chino Hills earthquakes are represented. The results of the present study seem to be in reasonable agreement with those from literature. The ranges estimated in this work generally increase with period, similarly to other studies (e.g. Jayaram and Baker 2009, Esposito and Iervolino 2011, 2012, Goda and Hong 2008). As highlighted by Jayaram and Baker (2009) and Esposito and Iervolino (2012), this is consistent with past studies on spatial coherency of ground motion (e.g. Zerva and Zervas 2002). Given that the coherency is a measure of similarity between two recordings, the aforementioned studies prove that this parameter decreases at increasing distance between two points and at higher frequencies. In fact, high-frequency waves are more affected by small-scale heterogeneities and therefore they turn out to be less coherent, compared to low-frequency waves (Kiureghian 1996). Regarding Figure 6, the results reveal different correlation decay rates. However, the high variability of the range values is comparable with that one found in literature works. The differences of the correlation structures among the different locations are mainly related to the frequency content of ground motion (e.g. Baker and Jayaram 2008 or Goda and Hong 2008a) and to peculiarities of the local geology and of the propagation path (Sokolov et al. 2010). Observing Figure 6, it can be noted that the ranges estimated for Po Plain, Istanbul and Beijing at short period (i.e. T = 0s and 0.2s) are similar (i.e. between 20-30 km) differently from Thessaloniki where the range turns out to be much higher (about 55 km). This may be a consequence of the local site conditions: most of the monitors selected in Thessaloniki are located on homogeneous hard rock with V_{S30}=2000 m/s (see top right of Figure 4) where the ground motion is expected to be more coherent. On the other hand, most monitors considered for the other three cases are located on highly variable ground conditions (Istanbul, bottom right of Figure 4) or deep soft soil (Po Plain and Beijing, left top and bottom right of Figure 4). In the latter case it should be also considered that, even if the soil conditions are homogeneous in term of $V_{S,30}$, the sediment depth is strongly variable, thus affecting ground motion variability. Differences in the range values are apparent especially at short period intensity measures, where site effects are expected to be more significant, while they become less significant at increasing periods.

Finally, it can also be noted that the ranges obtained from the Po Plain simulation at long periods are rather small compared to the other three locations, most likely because receivers in the Po Plain are all located at very short distances from the fault, where near-source effects are predominant, increasing the

variability of ground shaking.

5. CONCLUSIONS

This paper aims at demonstrating the capability of broad-band physics-based numerical simulation to reproduce the real spatial correlation structure of earthquake ground motion. Given that ground motion correlation structure is highly dependent on local geology and on the propagation path, a single generalized spatial correlation model may not adequately represent large areas, as shown by Sokolov et al. (2010) for the Taiwan case. Thus, the spatial correlation models proposed in literature, based on the analysis of large sets of strong motion recordings, can be hardly representative of all the possible situations. In this regard, this work highlights that 3D physics-based numerical simulations represent a powerful tool to cope with the aforementioned limitation and to provide a better understanding of the physical factors affecting the spatial variability of ground motion.
The spatial correlation of different response spectral ordinates was evaluated based on standard geostatistical tools, based on the computation of the semivariogram. From the semivariogram, the separation distance at which the spatial correlation can be considered lost, referred to as range, was computed. The numerical dataset analyzed in the present study includes four different regions worldwide, namely: Po Plain (Northern Italy), Thessaloniki (Northern Greece), Beijing (China) and Istanbul (Turkey). In each area a large set of synthetic broadband seismograms, usable in the entire frequency range of interest for engineering applications, was produced by means of physics-based numerical simulations coupled with artificial neural network technique (Paolucci et al., 2017). Additionally, for the Po Plain case study, a large set of high quality near source records is available. Hence, for this case study, it was possible to perform a validation study by comparing the spatial correlation structure reproduced by the simulation with the real one computed using the recorded strong motion data. Instead, for the other case studys, results from 3D simulations were compared with some previously published research studies based on ground motion observations.

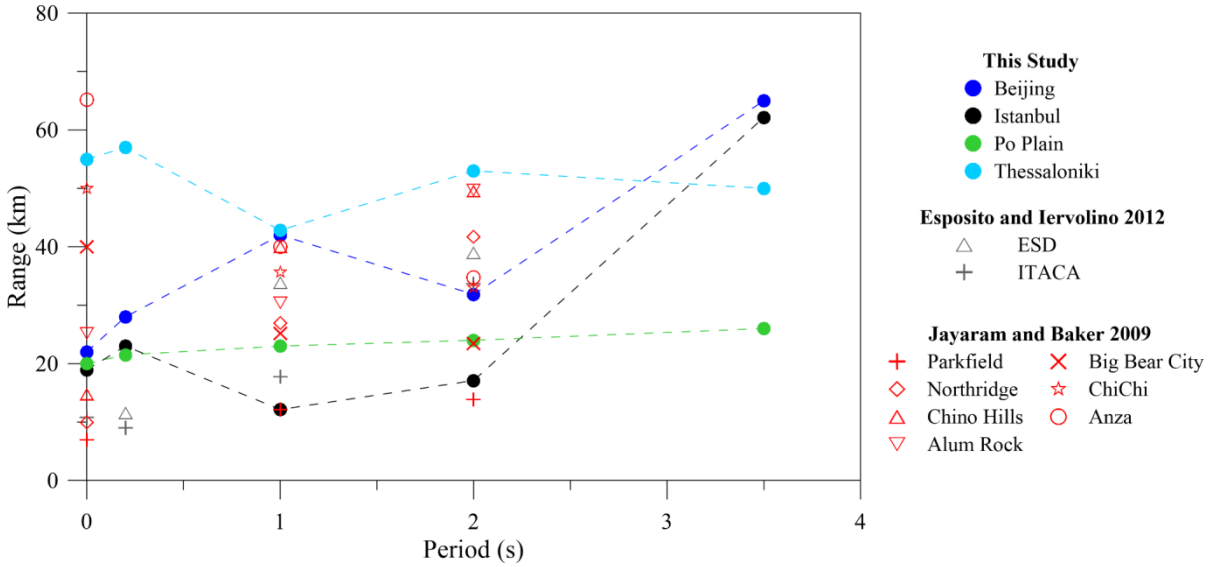

Figure 6. Comparison of the ranges estimated in this study against the results of Esposito and Iervolino (2012) and Jayaram and Baker (2009).

The most salient results can be summairzed as follows: (i) ranges estimated based on Po Plain simulation are consistent with the ranges based on real data recorded during Po Plain earthquake in 2012, demonstrating that numerical simulations can realistically represent the real correlation structures at long and short periods (Figure 2); (ii) overall, our range estimates are comparable with the available literature on the topic (Figure 6); (iii) however, these estimates shows a marked variability across the different case studies investigated, especially at short periods, consistently with independent works (Figure 6); (iv) such a variability in range values seems to be mainly related to the peculiarities of the local geology and of the near source conditions.

Provided that this work demonstrates the ability of the 3D broad-band simualtions to reproduce the actual correlation structure, future studies will address the systematic investigation of the effects of the following factors on spatial correlation structure of ground motion: (i) site conditions (homogeneous versus heterogeneous, rigid versus soft soil, effect of alluvial basins etc.); (ii) near-source conditions: influence of the distance from the source (near field versus far field), source-to-site azimuth and focal mechanism.

To conclude, this paper confirms and corroborates the strength of 3DPBNSs especially for those regions characterized by a limited or non-existent observational dataset where it is difficult to define a model able to describe the spatial correlation in a proper manner.

6. ACKNOWLEDGMENTS

This research activity has been carried in the framework of research projects funded by Munich RE (Germany), the 2014-2016 RELUIS RS2 Project funded by the Italian Department of Civil Protection and ISCRA and LISA projects.

7. REFERENCES

Antonietti P, Ferroni A, Mazzieri I, Paolucci R, Quarteroni A, Smerzini C, Stupazzini M (2017). Numerical Modeling of Seismic Waves by Discontinuous Spectral Element Methods. *Mox-Report,* 09/2017

Bao H, Bielak J, Ghattas O, Kallivokas L, O'Hallaron D, Shewchuk J, Xu J (1998). Large-scale simulation of elastic wave propagation in heterogeneous media on parallel computers. *Comput. Methods Appl. Mech. Engrg*., 152(1): 85 – 102.

Boore DM (2003). Simulation of Ground Motion Using the Stochastic Method. *Pure Appl. Geophys*., 160(3): 635–676.

Chaljub E, Maufroy E, Moczo P, Kristek J, Hollender F, Bard PY, Priolo E, Klein P, de Martin F, Zhang Z, Zhang W, Chen X (2015). 3-D numerical simulations of earthquake ground motion in sedimentary basins: testing accuracy through stringent models. *Geophys. J. Int.*, 201(1): 90–111.

Cressie, N, Hawkins DM (1980). Robust estimation of variogram, *Math. Geol.*, 12(2): 115–125.

Day SM, Graves R, Bielak J, Dreger D, Larsen S, Olsen KB, Pitarka A, Ramirez-Guzman L (2008). Model for basin effects on long-period response spectra in southern California. *Earthq. Spectra,* 24(1): 257–277.

Douglas J, Aochi H (2008). A Survey of Techniques for Predicting Earthquake Ground Motions for Engineering Purposes. *Surv. Geophys.,* 29(3): 187–220

Dumbser M., Käser M (2006). An arbitrary high-order discontinuous Galerkin method for elastic waves on unstructured meshes - II. The three-dimensional isotropic case. *Geophys. J. Int.,* 167(1): 319–336.

Esposito S, Iervolino I (2011). PGA and PGV Spatial Correlation Models Based on European Multievent Datasets. *Bull. Seismol. Soc. Am*., 101(5): 2532–2541

Esposito S, Iervolino I (2012). Spatial Correlation of Spectral Acceleration in European Data,. *Bull. Seismol. Soc. Am.,* 102(6) 2781–2788

Evangelista L, del Gaudio S, Smerzini C, d'Onofro A, Festa G, Iervolino I, Landolfi L,Paolucci R, Santo A, Silvestri F (2017) Physics-based seismic input for engineering applications: a case study in theAterno river valley, Central Italy. *Bulletin of Earthquake Engineering*, 15(7): 2645–2671

Gatti F, De Carvalho Paludo L, Svay A, Lopez-Caballero F, Cottereau R Clouteau D (2017). Investigation of the earthquake ground motion coherence in heterogeneous non-linear soil deposits. *X International Conference on Structural Dynamics*, EURODYN 2017, 10 - 13 September

Goda K, Atkinson GM (2009). Probabilistic characterization of spatially correlated response spectra for earthquakes in Japan. *Bull. Seismol. Soc. Am*., 99(5): 3003–3020.

Goda K, Atkinson GM (2010). Intraevent spatial correlation of ground-motion parameters using SK-net data, *Bull. Seismol. Soc. Am*., 100(6): 3055–3067.

Goda K, Hong HP (2008a). Spatial correlation of peak ground motions and response spectra. *Bull. Seismol. Soc. Am.*, 98(1): 354–365.

Graves RW (1996). Simulating seismic wave propagation in 3D elastic media using staggered-grid finite differences. *Bull. Seismol. Soc. Am.,* 86(4): 1091–1106.

Guidotti R, Stupazzini M, Smerzini C, Paolucci R and Ramieri P (2011) Numerical study on the role of basin geometry and kinematic seismic source in 3D ground motion simulation of the 22 February 2011 M_w 6.2 Christchurch earthquake. *Seismological Research Letters*, 82(6):767-782.

Hashemi K, Mazzieri I, Paolucci R, Smerzini C (2016). Spatial variability of near-source seismic ground motion

with respect to different distance metrics, with special emphasis on May 29 2012 Po Plain Earthquake, Italy,*7th International Conference on Seismology and Earthquake Engineering.*
Hong, HP (2000). Distribution of structural collapses and optimum reliability for infrequent environmental loads, *Struct. Saf.,* 22: 297–311.
Infantino M (2016) From 3D physics-based scenarios to advanced methods for seismic hazard assessment: the case of Istanbul. *Master Thesis in Environmental Engineering*, Politecnico di Milano.
Isbiliroglu Y, Taborda R, Bielak J (2015). Coupled Soil-Structure Interaction Effects of Building Clusters During Earthquakes. *Earthq. Spectra*, 31(1): 463-500.
Jayaram N, Baker JW (2009). Correlation model for spatially distributed ground motion intensities. *Earthq. Eng. Struct. Dynam*., 38(15): 1687–1708.
Journel AG, Huijbregts CJ (1978). Min. Geostat., *Academic Press*, London, 600 pp.
Der Kiureghian A (1996). A coherency model for spatially varying ground motions. *Earthquake Engineering and Structural Dynamics*, 25:99–111.
Komatitsch D, Tromp J (2002a). Spectral-element simulations of global seismic wave propagation-I. Validation, *Geophys. J. Int.,* 149(2): 390–412.
Komatitsch D, Tromp J (2002b). Spectral-element simulations of global seismic wave propagation-II. Three-dimensional models, oceans, rotation and self-gravitation, *Geophys. J. Int.,* 150(1) 303–318.
Loth C., Baker JW (2013). A spatial cross-correlation model of ground motion spectral accelerations at multiple periods. *Earthquake Engineering & Structural Dynamics*, 42(3):397-417
Mai PM, Beroza GC (2003). A hybrid method for calculating near-source, broadband seismograms: Application to strong motion prediction, *Phys. Earth Planet In.,* 137(1-4): 183–199.
Matheron G (1965). Les variables régionalisées et leur estimation, *Masso*n, Paris
Mazzieri I, Stupazzini M, Guidotti R, Smerzini C (2013). SPEED: SPectral Elements in Elastodynamics with Discontinuous Galerkin: a non-conforming approach for 3D multi-scale problems. *Int. J. Numer. Meth. Eng*., 95(12): 991–1010.
Olsen KB (2000). Site amplification in the Los Angeles basin from three-dimensional modeling of ground motion, *Bull. Seismol. Soc. Am.* 90(6B): S77–S94.
Paolucci R, Mazzieri I, Smerzini C (2015). Anatomy of strong ground motion: near-source records and 3D physics-based numerical simulations of the M_w 6.0 May 29 2012 Po Plain earthquake, Italy. *Geophysical Journal International,* 203(3): 2001–2020.
Paolucci R, Evangelista L, Mazzieri I, Schiappapietra E (2016). The 3D numerical simulation of near-source ground motion during the Marsica earthquake, central Italy, 100 years later. *Soil Dynamics and Earthquake Engineering*, 91: 39-52.
Paolucci R, Gatti F, Infantino M, Smerzini C, Özcebe AG, Stupazzini M (2017) Broad-band ground motions from 3D physics-based numerical simulations using artificial neural networks. *Bulletin of the Seismological Society of America* (submitted for review).
Park J, Bazzurro P, Baker JW. (2007). Modeling spatial correlation of ground motion intensity measures for regional seismic hazard and portfolio loss estimation. Tenth International Conference on Application of Statistic and Probability in Civil Engineering (ICASP10), Tokyo, Japan, 2007.
Pilz M, Parolai S, Stupazzini M, Paolucci R, Zschau J (2011). Modelling basin effects on earthquake ground motion in the Santiago de Chile basin by a spectral element code. *Geophysical Journal International*, 187(2): 929–945.
Pitarka A, Irikura K, Iwata T, Sekiguchi H (1998). Three-dimensional simulation of the near-fault ground motion for the 1995 Hyogo-Ken Nanbu (Kobe), Japan, earthquake, *Bull. Seismol. Soc. Am.,* 88(2): 428–440.
Sabetta F, Pugliese A (1996). Estimation of Response Spectra and Simulation of Nonstationary Earthquake Ground Motions, *Bull. Seismol. Soc. Am.,* 86(2): 337–352.
Smerzini C, Villani M (2012). Broadband numerical simulations in complex near-field geological configurations: the case of the 2009 M_w 6.3 L'Aquila earthquake. *Bulletin of the Seismological Society of America,* 102(6): 2436-2451.
Sokolov V, Wenzel F, Jean WY, Wen KL (2010). Uncertainty and spatial correlation of earthquake ground motion in Taiwan. *Terr. Atmos. Ocean. Sci*., 21(6): 905–921.
Smerzini C, Pitilakis K, Hashemi K (2017). Evaluation of earthquake ground motion and site effects in the Thessaloniki urban area by 3D finite-fault numerical simulations. *Bull Earthquake Eng*, 15(3): 787-812
Stupazzini M, Paolucci R, Igel H (2009). Near-fault earthquake ground-motion simulation in the Grenoble Valley by a high-performance spectral element code. *Bulletin of the Seismological Society of America*, 99(1): 286-301.
Taborda R, Bielak J (2014). Ground-motion simulation and validation of the 2008 Chino Hills, California, earthquake using different velocity models, *Bull. Seismol. Soc. Am*., 104(4): 1876–1898.
Tsuda K, Hayakawa T, Uetake T, Hikima K, Tokimitsu R, Nagumo H, Shiba Y (2011). Modeling 3D Velocity Structure in the Fault Region of the 2007 Niigataken Chuetu-Oki Earthquake with Folding Structuree, 4*th IASPEI/IAEE International Symposium-Effects of Surface Geology on Seismic Motion*, 1–11.

Villani M, Faccioli E, Ordaz M, Stupazzini M (2014). High-resolution seismic hazard analysis in a complex geological configuration: the case of Sulmona Basin in Central Italy. *Earthquake Spectra*, 30(4): 1801-1824.
Wald DJ, Graves RW (1998). The seismic response of the Los Angeles basin, California, *Bull. Seismol. Soc. Am.,* 88(2): 337–356.
Wang M, Takada T (2005): Macrospatial corrlation model of seismic ground motions. *Earthq. Spectra*, 21(4):1137-1156
Weatherill GA, Silva V, Crowley H, Bazzurro P (2015). Exploring the impact of spatial correlations and uncertainties for portfolio analysis in probabilistic seismic loss estimation. *Bull Earthquake Eng,* 13:957–981.
Zerva, A, Zervas V (2002). Spatial variation of seismic ground motion, *App. Mech. Rev*., 55(3): 271–297.